Increased Quantum Dot Loading by pH Control Reduces Interfacial Recombination in Quantum-Dot-Sensitized Solar Cells

Katherine E. Roelofs,[†] Steven M. Herron,[‡] and Stacey F. Bent*[,§]

[†]Department of Materials Science and Engineering, [‡]Department of Chemistry, and [§]Department of Chemical Engineering, Stanford University, Stanford, California 94305, United States

ABSTRACT The power conversion efficiency of quantum-dot-sensitized solar cells (QDSSCs) hinges on interfacial charge transfer. Increasing quantum dot (QD) loading on the TiO_2 anode has been proposed as a means to block recombination of electrons in the TiO_2 to the hole transport material; however, it is not known whether a corresponding increase in QD-mediated recombination processes might lead to an overall higher rate of recombination. In this work, a 3-fold increase in PbS QD loading was achieved by the addition of an aqueous base to negatively charge the TiO_2 surface during Pb cation deposition. Increased QD loading improved QDSSC device efficiencies through both increased light absorption and an overall reduction in recombination. Unexpectedly, we also found increased QD size had the detrimental effect of increasing recombination. Kinetic modeling of the effect of QD size on interfacial charge transfer processes provided qualitative agreement with the observed variation in recombination lifetimes. These results demonstrate a robust method of improving QD loading, identify the specific mechanisms by which increased QD deposition impacts device performance, and provide a framework for future efforts optimizing the device architecture of QDSSCs.

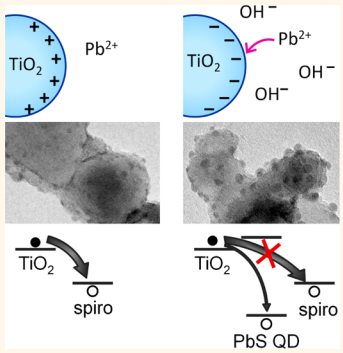

KEYWORDS: charge transfer · SILAR · lead sulfide · titanium dioxide · quantum dot · surface coverage · nanostructured solar cells

Dye-sensitized solar cells (DSSCs) have a highly modular architecture,[1] composed of a nanostructured metal oxide anode, sensitized with a light-absorbing dye, and infiltrated with a hole-transport material (HTM). The DSSC device structure has served as the basis for other solar cell architectures due to the ease of exchanging any given component, such as the electron-transporting anode, the absorber, or the HTM.[2] Quantum-dot-sensitized solar cells (QDSSCs) are an attractive variation on DSSCs, in which the monolayer of dye molecules is replaced by a single layer of quantum dots (QDs) as the absorber.[3−6] QDs are semiconductor nanocrystals with sizes small enough to fall in the quantum-confined regime, and have drawn interest as a next-generation absorber material.[7] One benefit is that the QD band gap varies with size, allowing the absorption onset to be tuned while employing the same absorber material, simply by changing the nanocrystal size. QDs have higher absorption coefficients and potentially greater stability than high-performance dye molecules.[7,8] Due to their size-dependent band gap, QDs of semiconductor materials with bulk band gaps below 1 eV can have the nanocrystal band gap tuned by quantum confinement to harvest the optimal range of photons from the solar spectrum, whereas it remains difficult to synthesize dye molecules with low-energy absorption onsets, since extensive conjugation is required.[7] Typically, the nanostructured metal oxide anode employed in QDSSCs is TiO_2, and promising metal chalcogenide QD materials for high-efficiency QDSSCs include CdS,[9] CdSe,[10] CdTe,[11] PbS,[12] $CuInSe_xS_{2-x}$,[13,14] In_2S_3,[15] and Sb_2S_3.[16] Despite the promising optical properties of QDs, QDSSCs have reached record efficiencies of only 8.6%,[17] still lagging behind the efficiencies of 12.3% in DSSCs.[18]

QDSSCs are part of an overall trend in the field toward inorganic-absorber, all-solid-state devices.[2,19] Replacing the organic dye molecules with inorganic absorbers in

* Address correspondence to sbent@stanford.edu.

Received for review May 11, 2015 and accepted July 28, 2015.

Published online August 05, 2015
10.1021/acsnano.5b02853

© 2015 American Chemical Society

DSSC-inspired architectures has led to the development of QDSSCs, extremely thin absorber (ETA) solar cells,[20] and, most recently, perovskite solar cells.[21−24] A solid-state device architecture refers to the replacement of the traditional liquid electrolyte with solid-state HTMs, *e.g.*, ionic species such as CuSCN[25] or organic semiconductors such as spiro-OMeTAD (2,2′,7,7′-tetrakis(*N*,*N*-di-*p*-methoxyphenylamine)-9,9′-spirobifluorene).[26] Employing solid-state HTMs avoids problems of leakage or corrosion of the absorber that can occur with liquid electrolytes.[27] The use of liquid electrolytes is a real and significant barrier to commercialization in these devices.[28] Photovoltaic technologies for utility power generation need lifetimes approaching 25 years to compete with the cost of grid electricity; even for technologies like QDSSCs with potentially lower materials costs, the balance of system cost is still high.[29,30] As can be seen from the example of disposable batteries, the issues associated with liquid electrolytes will limit device lifetimes.[31] Moreover, nonutility applications of QDSSCs, such as portable or flexible solar cells, typically involve direct use by consumers for which the safety concerns of liquid electrolytes are a problem. This is especially true for flexible solar cells, where low-cost encapsulation techniques will be a challenge.[32]

However, the incorporation of a solid-state HTM introduces new challenges; a major issue is reducing charge recombination at the anode/QD/HTM interface and improving charge transport to the electrodes. These effects are especially critical in devices with solid-state HTMs, which have more severe rates of recombination relative to liquid electrolytes[27,33,34] and lower mobilities.[35] Due to these issues, solid-state QDSSCs have reached device efficiencies of only 1.5%,[36] and the majority of research in the field is on QDSSCs with liquid electrolytes. We believe that for commercialization of QDSSCs the issues in solid-state devices need to be solved and that one of the first challenges to tackle is to decrease interfacial recombination in these devices. A common approach used to decrease recombination is to modify the QD absorber or TiO_2 anode, *e.g.*, through increased QD loading of the TiO_2 surface, doping of the QDs to optimize interfacial band alignment, or deposition of additional materials such as insulating metal oxide layers at the TiO_2 surface.[2]

Increasing QD coverage strikes at the heart of a primary problem in the QDSSC design: QDSSCs struggle to achieve high QD loading.[37−39] While DSSCs realize nearly complete dye coverage of the TiO_2,[40−43] QD coverage of 15% of the TiO_2 surface is high for QDSSCs,[44] with, for example, only 6% coverage achieved in the highest-efficiency ss-QDSSCs.[36] Increased QD deposition has the clear benefit of increased absorption; previous studies on *in situ*[45,46] and *ex situ*[44] synthesized QDs indicate that increased QD deposition increases external quantum efficiency (EQE), which the authors attributed to increased adsorption. Bare regions of the TiO_2 surface, not covered by an absorber, contribute significantly to recombination due to the close proximity to the HTM.[47] Increasing QD loading could prevent recombination by limiting exposed TiO_2 surface. In the DSSC system, increases in dye coverage have been found to have a positive effect on electron lifetimes, through the suggested mechanism of blocking recombination from the TiO_2 to the HTM.[48] In QDSSCs, such a beneficial effect of increased absorber coverage cannot be assumed, as interfacial charge transfer is expected to be significantly different.[39] For instance, in some of the highest-performing dye molecules, after electron transfer the HOMO orbital of the dye molecule (where the hole is localized) is shifted away from the TiO_2 surface, thus helping to decrease recombination of TiO_2 electrons with the dye cation.[49] Conversely, QDs introduce multiple new recombination pathways, due to defects and trap states at the TiO_2/QD interface, through which TiO_2 electrons can recombine with holes in the QD or in the HTM. In fact, studies have shown in a few systems that the rate of QD-mediated recombination is higher than that of TiO_2 electrons directly recombining with the HTM (*i.e.*, through bare regions on the TiO_2 surface).[47,50] Other studies suggest that while recombination to the HTM dominates initially, there is a regime change to favor QD-mediated recombination at higher deposition cycles of the QD.[51] Accordingly, it is not obvious if increasing QD loading will decrease or increase the loss of photocurrent due to recombination.

QDSSCs can be fabricated by the *ex situ* synthesis of QDs *via* colloidal methods or by the *in situ* growth of QDs directly on the anode surface. QDs synthesized by *ex situ* methods can be infiltrated into the nanoporous TiO_2 substrate by simply soaking in a suspension of colloidal QDs,[52,53] by employing linker molecules to attach the QDs to the TiO_2,[54−56] or by electrophoretic deposition.[57,58] Despite this variety of infiltration techniques, the *ex situ* method gives lower QD loading than *in situ* QD growth, because it relies on the infiltration of preformed QDs into the nanostructured anode, rather than the infiltration of the chemical precursors for QD growth.[6] *In situ* QD growth techniques include chemical bath deposition (CBD),[59,60] atomic layer deposition (ALD),[61−63] and, perhaps the most common technique, successive ion layer and adsorption reaction (SILAR).[36,64] In one SILAR deposition cycle, the anode is first dipped in a solution containing the metal cation precursor, followed by a rinsing step, and then the anion precursor solution, with a final rinse. Additional SILAR cycles can introduce two types of deposition: the continued growth of existing nanocrystals or the nucleation of new nanocrystals.[64,65] A fairly broad distribution of QD sizes is characteristic of the SILAR process.[36,64,66]

Several approaches have been taken to improve QD nucleation and growth on the TiO_2 anode during SILAR. An intrinsic difficulty with SILAR deposition on nanoporous substrates is that the precursor ions easily

reach and deposit on the outer region of the nanoporous film, but have a more difficult time diffusing into the interior region of the film. Thus, at higher SILAR cycles, QDs growing on the outer region of the TiO_2 film can actually block the pore channels to the inner regions, hindering any further QD nucleation on the interior.[67,68] This phenomenon is referred to here as pore-blocking. Strategies to improve the ion transport to and reaction with the anode surface include potential-induced solution deposition techniques,[69] improving the wetting of precursor solutions on the anode surface,[36] and sulfidizing the anode (for better growth of metal sulfide QDs).[70] A recent study by Park and colleagues focused on Hg-doped PbS QDs and found that adding a base to the Pb^+ cation solution increased QD loading.[71] The authors hypothesize that the lower pH of the cation precursor solution causes the TiO_2 surface to be negatively charged, encouraging the adsorption of Pb cations and leading to the observed increase in QD loading.

In this work we use base-assisted SILAR deposition to investigate the impact of increased PbS QD loading on device performance, with particular focus on the impact of QD coverage of the TiO_2 surface on interfacial recombination. We demonstrate a robust method of improving initial QD loading through the use of three different bases, NaOH, ethylenediamine (ED), and triethanolamine (TEA), and examine the mechanism by which the addition of a base to the cation precursor solution influences QD deposition. The QD-coated films are used to fabricate solid-state QDSSCs with spiro-OMeTAD as the HTM, since in solid-state devices decreasing interfacial recombination is of even greater importance than in devices with liquid electrolytes. Increased QD coverage is shown to increase recombination lifetimes by over an order of magnitude, revealing the beneficial impact of higher QD loading. The effects of increased QD deposition are complicated by the variation in both the number of QDs and the QD size with increased SILAR cycles; increased QD size is found to decrease recombination lifetimes. The effect of changing QD size, *i.e.*, QD band gap, is modeled based on the expected change in rate constants with shifts in the QD band energy levels, providing a potential explanation for the observed trend in recombination lifetimes. While previous studies have reported recombination in CdSe[51,72] and PbS[73] QDSSCs as a function of SILAR cycle, this is the first work to combine recombination measurements with a technique to significantly enhance QD loading without further deposition cycles. This has provided the new insight that two opposing effects are at play with QD deposition in this system: higher QD loading reduces recombination, while increased QD size can actually increase interfacial recombination.

RESULTS AND DISCUSSION

QD Characterization. We first characterized the lead(II) sulfide QD growth as a result of adding different bases

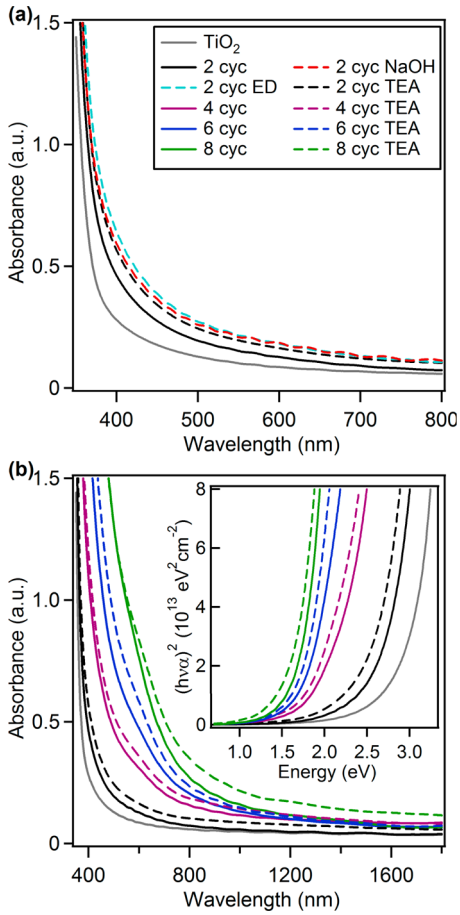

Figure 1. UV−vis spectroscopy of nanoporous TiO_2 films sensitized by PbS QDs. Shown are (a) blank TiO_2 films and 2 SILAR cycles of QDs grown by the standard process (solid line) and in the presence of NaOH, ED, and TEA (dashed lines). Also shown (b) is the trend with 2, 4, 6, and 8 SILAR cycles comparing the standard process and TEA-assisted QD growth, with the corresponding Tauc analysis curves shown in the inset.

to the cation solution during SILAR; NaOH, ED, and TEA were explored. In each case, the concentration of the base in the aqueous $Pb(NO_3)_2$ solution was adjusted to reach a pH of 9 (for TEA the pH was 9.2). Figure 1a plots the UV−vis absorption measurements of QD-coated nanoporous TiO_2 films in which 2 SILAR cycles of QDs are grown with the addition of NaOH, ED, TEA, or by the standard process. In terms of the absorption response, all three bases were found to increase PbS deposition to a similar extent.

Figure 1b tracks the progression in the UV−vis spectra with increasing SILAR cycles, comparing the standard process to the case of TEA. The analogous UV−vis spectra for NaOH and ED with increasing SILAR cycles are shown in Supporting Information Figure S1 and match that of TEA at a given cycle. In all cases, increasing the number of SILAR cycles leads to absorption onset at longer wavelengths. This demonstrates the quantum effect that increasing the QD size decreases the band gap, until bulk conditions are approached, although we note that higher QD loading causing

stronger absorption or aggregation of the QDs can also contribute to the apparent shift in absorption onset. PbS is a desirable QD absorber material, as it has a large Bohr exciton radius (18 nm) and confinement occurs up to a relatively large QD radius, permitting greater control over the band gap for a given change in radius. The bulk band gap of PbS is 0.37 eV, and confinement increases the band gap through the optimal point of interest for capturing the solar spectrum (~1.1 eV). The UV–vis results show at each SILAR cycle an increased absorption for QDs grown with TEA compared to those grown without. To isolate the effect of QD size, the inset in Figure 1b plots the Tauc analysis of the UV–vis spectra, from which the QD band gap was determined for each condition (Supporting Information Table S1). We note that the Tauc analysis of these substrates is susceptible to interpretation as to where the tangent line is drawn due to the extended curvature of the absorption onset, which is caused both by the distribution in QD size (and thus band gap) in a given substrate and by sub-band-gap absorption from defect states in the QDs. Therefore, the band gaps extracted from the Tauc analysis should be taken as nominal values indicative of trends rather than absolute values. The QD diameters expected for these band gaps, as calculated through band gap/size calibration curves for PbS QDs found in the literature, can be found in the Supporting Information (Table S1).[74] Higher band gaps are observed with TEA, indicating that the increased absorption at a given SILAR cycle is due at least in part to a shift toward an earlier absorption onset from larger QDs. A greater number of QDs may also be present, but this cannot be determined conclusively from the UV–vis results.

To directly observe the impact of high-pH cation solution on QD nucleation and growth, samples from QD-sensitized nanoporous TiO_2 films were examined by TEM. Representative TEM images are shown in Figure 2, with the extracted QD size and coverage summarized in Figure 3. The PbS QDs are shown by HRTEM (Supporting Information Figure S2) to be in the rocksalt crystal structure, and that near-stoichiometric PbS is indeed deposited is further confirmed by Auger electron spectroscopy analysis presented below. A rough calculation of absorbance as predicted from the TEM loading, using literature extinction coefficient values for PbS, matches the absorbance measured in the UV–vis data (see Supporting Information). At 2 SILAR cycles, increased QD loading and larger QDs were observed for NaOH, ED, and TEA, as compared to the standard process. TEM images were analyzed to determine the portion of the TiO_2 surface area covered by QDs, as well as the average QD diameter for each condition, shown in Figure 1. There is a fair match between the QD size extracted from the Tauc analysis of the UV–vis spectra and the average QD size observed in TEM (Table S1), although we note that TEM measurements of QD size are more reliable than band gaps extracted from UV–vis spectra due to the intrinsic difficulties of Tauc analysis of nanocrystals, discussed above. However, it is encouraging that the bulk measurement technique of UV–vis spectroscopy and the inherently local sampling technique of TEM are in agreement here.

Tracking the continued deposition in the case of TEA, higher QD loading is still apparent at 4, 6, and 8 SILAR cycles, although the effect diminishes with increasing SILAR cycles and is close to the range of error by 6 cycles. The diminished gains in coverage with TEA at higher SILAR cycles seem to indicate a self-saturating process, in which QD deposition has an upper limit that is approached by the TEA-assisted growth sooner than by the standard process. The self-saturation in QD growth could be due to pore-blocking, as discussed above, or due to epitaxial growth of the QDs, where the nanocrystal size limit is ultimately determined by any lattice mismatch between the TiO_2 substrate and the QD.[73] Another possible explanation for the saturation of QD growth is that once some QDs are nucleated in the first cycle or two, additional Pb^{2+} and S^{2-} adsorption

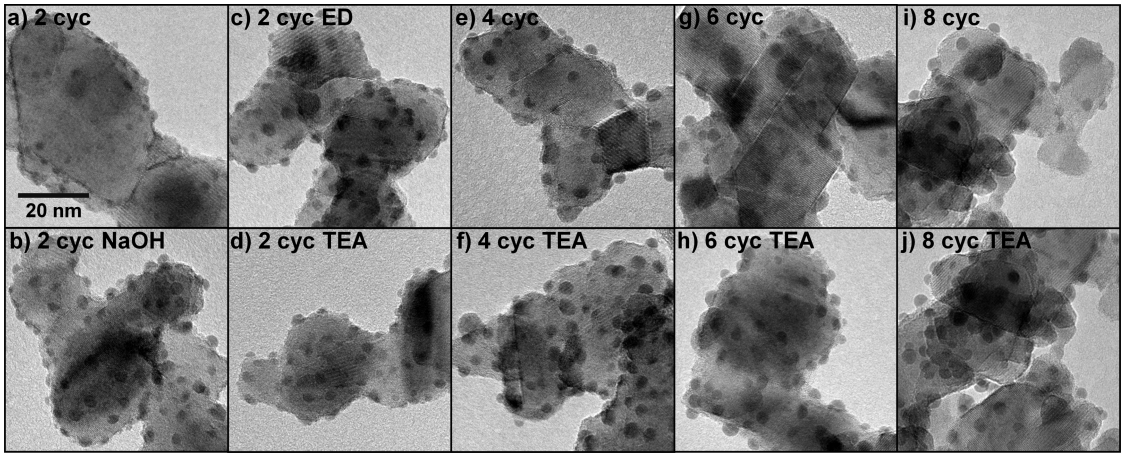

Figure 2. Representative TEM images of PbS QDs grown on TiO_2 nanocrystals, at the same magnification. Shown are 2 SILAR cycles comparing (a) the standard process with that with (b) NaOH, (c) ED, and (d) TEA. Also shown are higher SILAR cycles by (e, g, and i) the standard process and (f, h, and j) that with TEA.

occurs on the already nucleated QDs, which may be the case if PbS strongly prefers to grow on itself over TiO_2. Overall, the largest gains in QD coverage of the TiO_2 surface with base-assisted growth were seen initially at 2 SILAR cycles, and each of the three bases investigated produced similar gains in the number and size of QDs.

Figure 4 shows Auger electron spectroscopy (AES) line scans of the cross-section of TiO_2 films infiltrated with PbS QDs grown by the standard SILAR process as compared to that with TEA-assisted growth; the raw intensity data are included in the Supporting Information Figure S3. The AES line scans confirm the TEM and UV−vis results that base-assisted QD growth gives a higher QD loading, with roughly twice as much Pb and S as in the standard process. In both cases, higher amounts of Pb can be observed near the TiO_2 film surface, indicating QD growth is indeed faster at the top of the film.

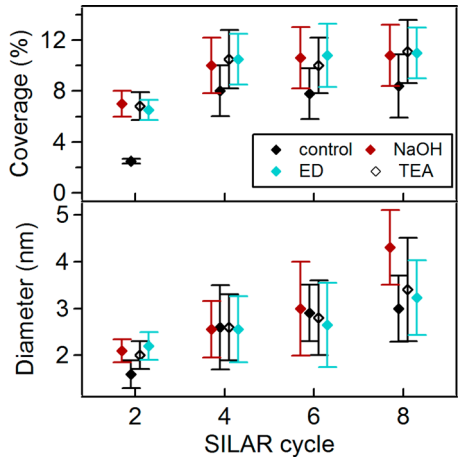

Figure 3. PbS QD size and loading calculated from TEM images, showing the average QD diameter and percent of the TiO_2 surface area covered by QDs. QDs were deposited for varying SILAR cycles by the standard process and with NaOH-, ED-, and TEA-assisted growth. At each SILAR cycle the points are staggered for visibility. Six TEM images were analyzed for each sample, corresponding to roughly 0.03 μm^2 of TiO_2 surface area and 300 QDs; error bars show the standard deviation.

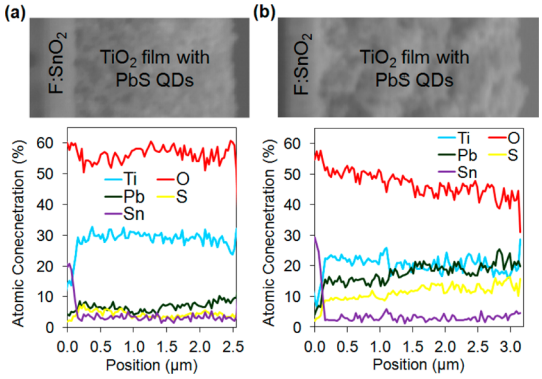

Figure 4. Auger electron spectroscopy line scan of sample in cross-section for nanoporous TiO_2 films on FTO, sensitized with 6 SILAR cycles of PbS QDs grown (a) by the standard process and (b) with TEA. Shown are the atomic concentrations; the raw intensities are included in Supporting Information Figure S3.

The mechanism by which the addition of a base increases the nucleation and growth of QDs on TiO_2 is not obvious. Park and coworkers propose that TEA could increase Pb^{2+} adsorption by negatively charging the TiO_2 surface.[71] The 0.02 M $Pb(NO_3)_2$ aqueous solutions have a pH of 4.3, while the pristine point of zero charge of anatase TiO_2 in aqueous solutions occurs at a pH of ~6.[75] Therefore, adjusting the cation solution to a pH of 9 should change the TiO_2 surface charge from positive to negative. In addition to affecting the TiO_2 surface charge, TEA is a chelating agent that can complex with the Pb^{2+} ions in the aqueous $Pb(NO_3)_2$ solution. Thus, TEA can lower the concentration of free Pb^{2+} in solution (although this would be expected to decrease, not increase, PbS deposition). Further, TEA can be chemisorbed or physisorbed on the surface of TiO_2, which could affect the transfer of Pb^{2+} from the bulk solution to Helmholtz layers immediately above the TiO_2 surface. Employing NaOH and ED bases allows us to separate out these effects. NaOH will not act as a chelating agent to complex with Pb^{2+} nor adsorb to the TiO_2 surface, so it is expected to purely affect the TiO_2 surface charge. Like TEA, ED can adsorb on the TiO_2 surface, but ED is only a bidentate chelating agent, while TEA is a tridentate chelating agent. From the UV−vis results (Figure 1 and Figure S1) and TEM results (Figure 2 and Figure 3), it can be seen that the use of NaOH or ED to adjust the $Pb(NO_3)_2$ solution to a pH of 9 leads to similar gains of QD nucleation and growth to those achieved with TEA. The common factor between these three bases is the shift in the solution pH; therefore we conclude that the increased PbS deposition is due to electrostatic effects rather than side chemical reactions. In addition, we have demonstrated a robust method to achieving increased QD loading through the use of different bases. This method is applicable to the deposition of other QD absorbers, such as Sb_2S_3 and In_2S_3, in which, depending on the particular cation salt used, the cation solutions have pH < 6.[64]

Device Performance. Figure 5 plots the photovoltaic performance (J−V curves) of champion solid-state QDSSCs fabricated with PbS QDs deposited under varying conditions; the average performance metrics for each condition are shown in Figure 6 and listed in Supporting Information Table S2. At 2 SILAR cycles (Figure 5a), there are dramatic gains in power conversion efficiency (PCE) for the case of NaOH, ED, and TEA, through gains in both short-circuit current (J_{SC}) and open-circuit voltage (V_{OC}). For ease of viewing, the J−V curves for higher SILAR cycles with TEA are shown in Figure 5b−d as a representative case, with the same data for NaOH and ED in Supporting Information Figure S4. Comparing NaOH, ED, and TEA to the standard deposition process at 2 SILAR cycles, the 3 to 3.5-fold gain in J_{SC}'s observed with base-assisted growth is on the same

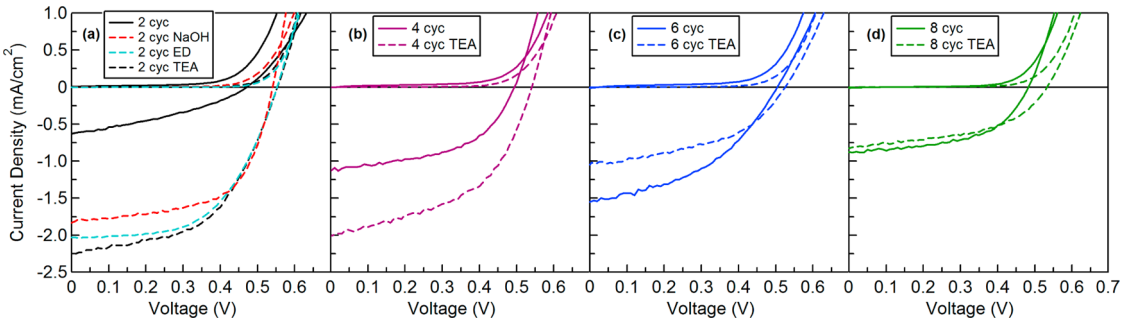

Figure 5. Current−voltage (J−V) curves showing the performance under 1 sun illumination and in the dark of the highest-performing devices at each QD deposition condition.

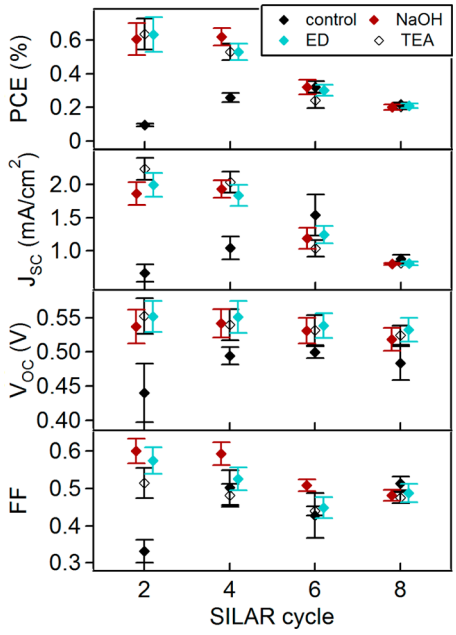

Figure 6. Average device parameters—power conversion efficiency (PCE), short-circuit current (J_{SC}), open-circuit voltage (V_{OC}), and fill factor (FF)—for varying QD SILAR deposition cycles, by the standard process (control), as well as NaOH, ED, and TEA-assisted growth. At each SILAR cycle, the points are staggered for visibility. Device parameters were averaged from 10 devices (the two best cells from five different substrates), and error bars represent standard deviations. Corresponding values are listed in Table S2.

order as the 2.6−2.8-fold gains in QD coverage of TiO_2 (Figure 3), suggesting that the increased light absorption from higher QD loading could be a significant contributor to the increased current collected. Although increased absorption does not ensure the charges are collected, our recombination studies (see below) suggest charge collection improves as well. While the device efficiency for the standard process peaks at 6 SILAR cycles, the highest efficiency for NaOH and TEA were observed at 2 cycles and for ED at 4 cycles (though 2-cycle ED had efficiencies close to 4-cycle ED). At a given deposition cycle, devices with base-assisted growth had dark current curves shifted outward to higher voltages and higher V_{OC} values than the standard devices. Outward-shifted dark curves and higher V_{OC} values are consistent with decreased recombination. The efficiency

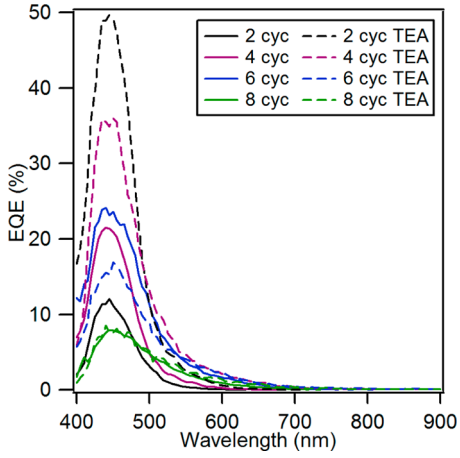

Figure 7. External quantum efficiency (EQE) spectra measured at short circuit of the highest-efficiency devices with increasing SILAR cycles of PbS QDs compared for the standard process (solid lines) and that with TEA (dashed lines).

for our best device, 2-cycle TEA, is 0.65%, while the record device efficiency for solid-state QDSSCs is 1.5%.[36]

To better understand the impact of variations in QD deposition on device performance, we measured the devices' EQE. EQE measurements can shed light on the contribution of different-sized QDs to the J_{SC} in a given device. Figure 7 plots the EQE spectra for increasing SILAR cycles of the standard devices compared to TEA. The EQE data match the trend in J_{SC}, although integration of the EQE spectra gives expected J_{SC} values that are roughly 20% lower than the J_{SC} values from the J−V curves (see Supporting Information Table S3, Figure S5, and discussion). The main observation from the EQE data is that, although there are some differences due to the broadening of the QD size distribution, the improvements in the J_{SC} with TEA appear to be dominated by the increase in the number of QDs at a given size. For instance, at 2 SILAR cycles, the EQE spectra for the TEA device have a similar distribution over wavelength to that of the standard device, just with higher values, indicating that QDs of a similar size range are contributing in each case, with a greater number of QDs present with TEA.

It might be expected that larger QDs would shift the EQE spectra toward longer wavelengths. However,

even comparing the 8-cycle and 2-cycle standard devices, there is only a slight skewing of the EQE spectra toward longer wavelengths for 8 cycles. Most strikingly, the EQE spectra remain quite narrow at higher SILAR cycles despite the shift in QD absorption onset to longer wavelengths observed in the UV–vis spectra. Thus, while there is strong absorption from QDs with band gaps of $\lesssim$2 eV (absorption onsets $\gtrsim$600 nm), for instance in the 8-cycle standard device as seen in Figure 1, these QDs are not contributing to charge collection. It could be that at less than 2 eV the PbS QD band gap is not large enough to properly align the QD conduction band with that of TiO_2 for transfer of the excited electron and the QD valence band with the spiro-OMeTAD HOMO level for hole transfer, or it could be that there is not enough of an energetic overpotential for efficient electron injection into the TiO_2[76] or hole transfer to the spiro-OMeTAD.[77] This result is similar to a previous report in a TiO_2/PbS QD/spiro-OMeTAD device that band gaps greater than 1.55 eV were required for effective charge splitting.[36] Therefore, increased device efficiency hinges on increased initial QD nucleation, such that many small QDs can be introduced with the correct band gap level.

Interfacial Recombination. We are interested in determining the effect of increased QD coverage of the TiO_2 surface on recombination at the TiO_2/HTM interface. Transient photovoltage measurements allow us to measure the recombination lifetimes of electrons leaving the TiO_2 at the interface; longer electron recombination lifetimes (τ_n) correspond to decreased rates of recombination. Figure 8 plots the recombination lifetimes measured for the same set of devices in Figure 5. Recombination lifetimes are plotted against V_{OC}, the open-circuit voltage values at which they were measured. Representative raw transient photovoltage decay curves are shown in the Supporting Information Figure S6. We confirmed that there is no shift in the TiO_2 conduction band level between different devices by measuring the transient photocurrent decay for the same light pulse flux densities as the transient photovoltage decay set points. By integrating the photocurrent decay, the charge density shift corresponding to the voltage shift in the transient photovoltage measurements can be found. For the set of devices in this study, the charge density *versus* voltage plots were identical. Therefore, TiO_2 conduction band shifts can be ruled out as a cause of the change in recombination lifetimes.

In Figure 8a, the recombination lifetimes at 2 SILAR cycles for the standard process are compared to QDs grown with NaOH, ED, and TEA. We observe an order of magnitude change toward longer recombination lifetimes with each of the bases, as compared to the standard process. When considering the physical differences in the QDs between these samples, this data set highlights the large change in surface coverage at 2 SILAR cycles, with 2.5% QD coverage of the TiO_2 surface for 2 SILAR cycles by the standard deposition and coverages of 7.0%, 6.5%, and 6.8% achieved with

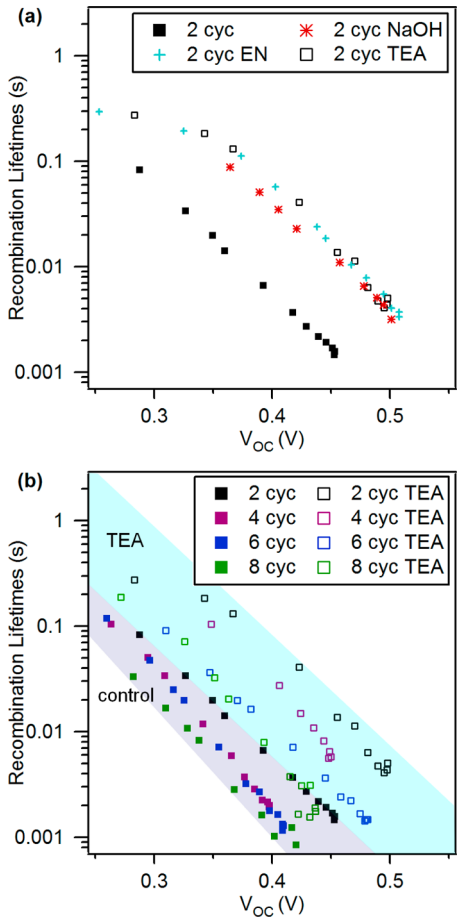

Figure 8. Recombination lifetimes comparing (a) 2 SILAR cycles of QDs grown by the standard process and in the presence of NaOH, ED, and TEA. (b) Recombination lifetimes of 2, 4, 6, and 8 SILAR cycles comparing the standard process and TEA-assisted QD growth. To guide the eye, the purple band highlights the standard process (control), and the light blue band highlights the TEA data points.

NaOH, ED, and TEA, respectively. We note that effects of increased coverage are convoluted with any effects due to the shifting QD band gap, as the base-assisted growth also gives larger QDs (from 1.6 nm diameter QDs by the standard process to 2.1, 2.2, and 2.0 nm with NaOH, ED, and TEA, respectively). However, we observe in Figure 8b that increasing QD size is correlated with shorter recombination lifetimes (see discussion below). Accordingly, we attribute the longer recombination lifetimes with base-assisted QD growth in Figure 8a to the increased QD loading. At higher QD loading, the overall effect is longer lifetimes, demonstrating that the beneficial effects of the QD, such as blocking TiO_2-to-HTM recombination, outweigh any harmful effects, such as participation in QD-mediated recombination processes. We note that studies reporting higher rates of QD-mediated recombination than TiO_2-to-HTM recombination (which suggests that more QDs would have an overall harmful effect) were conducted with liquid electrolytes.[47,50,51] Together, the longer recombination lifetimes, outward shift in the dark current J–V curves,

and higher V_{OC}'s all indicate decreased recombination in the devices with base-assisted QD growth, particularly at 2 SILAR cycles. Our results highlight that in QDSSCs with solid-state HTMs, which have faster rates of TiO_2-to-HTM recombination than liquid electrolytes,[27,33,34] increasing the QD loading leads to overall benefits in decreased recombination.

It is difficult to separate the impact of increased coverage of the TiO_2 surface from that of increased QD size, because changing deposition parameters normally affects both. In this work, we are able to substantially change QD surface coverage with base-assisted QD growth and compare those results to the standard SILAR growth process. However, due to the slight differences in QD size between base-assisted growth and standard growth (Figure 3), there were only a few data points that had identical QD sizes but different surface coverages. However, holding surface coverage constant, we were able to see the effects of varied QD size by comparing samples grown with TEA at 4, 6, and 8 SILAR cycles, where QD diameter increases substantially (from 2.6 to 3.2 nm) but surface coverage remains roughly constant (10.5 to 11.1%). From Figure 8b, it can be seen that moving from 4 to 6 to 8 SILAR cycles with TEA leads to shorter recombination lifetimes. From this, we conclude that increasing QD size increases the rate of recombination. Nevertheless, for each number of SILAR cycles studied, the use of TEA consistently helps increase recombination lifetimes and, as discussed above, we attribute this effect to blocking of TiO_2-to-HTM recombination by the QD layer.

A possible mechanism by which increasing QD size could decrease recombination lifetimes is that the rise of the QD valence band that occurs as the band gap shrinks could hinder hole transfer from the oxidized QD to the spiro-OMeTAD. Hindering this hole transfer, which regenerates the QDs to a neutral charge state, would leave more QDs in the oxidized state and increase the rate of recombination (which is dependent on the recombination rate constant and the concentration of oxidized QDs) from the TiO_2 conduction band to oxidized QDs. The rate of hole transfer for QD regeneration has recently been shown to have a significant impact on device performance. Regeneration rates have been measured at microsecond time scales,[36] while the initial electron injection in QDSSCs with *in situ* grown QDs occurs on the picosecond time scale or faster,[3,78−80] although we note that there are recent reports of QDSSCs with *ex situ* grown QDs in which electron injection has been reported on the nanosecond time scale.[81] Due to the sensitivity of device performance to the QD regeneration step, we suggest slow hole transfer for QD regeneration as a likely mechanism by which decreasing the QD band gap increases the rate of recombination. This proposed mechanism is further supported by previous literature experiments showing a decrease in the yield of hole transfer from PbS QDs to spiro-OMeTAD for PbS QDs larger than 2.5 nm; the authors also observe a faster decay of the spiro-OMeTAD cation with increasing QD size, leading them to conclude that the hole can be back-transferred from the spiro-OMeTAD cation to the QD if the QD valence band shifts to high enough energy levels.[36]

Our observed result of shorter recombination lifetimes with increased SILAR cycles runs contrary to previous reports on recombination in CdSe[51,72] and PbS[73] QDSSCs. In the report on PbS QDs on SnO_2 substrates, Cánovas and colleagues found that recombination lifetimes increased from 2.6 to 8.1 ns from 1 to 3 SILAR cycles,[73] using optical pump−terahertz probe spectroscopy that focuses on the short-range recombination processes, which the authors attribute to recombination to oxidized QDs. Our results are not directly comparable, as we are measuring small-perturbation recombination processes with resolution limited to the microsecond time scale; recombination lifetimes at the TiO_2/spiro-OMeTAD interface determined by transient photovoltage measurements are typically 100 to 1000 μs.[82] In addition, we studied a larger size range of the PbS QDs, from 2 to 8 SILAR cycles, and on the standard TiO_2 substrate. For CdSe QDs, Bisquert and colleagues have found that recombination lifetimes are longer with increasing SILAR cycles, which the authors attribute to the QDs blocking recombination from the TiO_2 to the HTM. They further report that recombination lifetimes do not significantly change with increasing SILAR cycles of CdS QDs.[51] The difference in our results could be due to our use of PbS QDs; increasing QD size approaches the PbS bulk band gap of 0.37 eV, whereas CdSe has a bulk band gap of 1.7 eV. Accordingly, the valence band edge of PbS QDs can rise quite significantly, compared to CdSe or CdS QDs, making hole transfer from the QD to the HTM more difficult in the case of PbS QDs, in keeping with the mechanism proposed above. A range of QD materials with varying bulk band gaps would need to be studied in future work to determine if this accounts for the difference.

Our result of shorter recombination lifetimes with higher SILAR cycles was unexpected; accordingly, we have further investigated this effect with a model, to see if the proposed mechanism could produce the observed trend in recombination lifetimes. We modeled the dependence of the recombination lifetime on the QD valence band level. The measured recombination lifetime, τ_n, has components due to two main sources of recombination at the interface: electrons in the TiO_2 conduction band recombining with the oxidized QD giving a lifetime τ_{r1} or with holes in the spiro-OMeTAD giving a lifetime τ_{r2} (eq 1). This model is based on the treatment put forth by O'Regan, Miettunen, Grätzel, and colleagues in their review on optoelectronic measurements in DSSCs.[83] The transient photovoltage measurements above track only the recombination of

photoelectrons already injected into the TiO_2 that are now leaving the TiO_2 *via* recombination. As such, the ultimate recombination destinations of the TiO_2 electrons in QDSSCs are the same as DSSCs: the electron will recombine with a hole in the absorber (the QD) or a hole in the HTM. However, the approach put forth by O'Regan *et al.* for DSSCs is further complicated when applied to QDSSCs, due to the presence of defects at the TiO_2/QD interface, which can act as trap states, delaying or facilitating electrons leaving the TiO_2 to ultimately reach the QD or the HTM. Therefore, for simplicity of approach, we assume that the additional complications of trap states can be incorporated into the recombination time constants for recombination to the QD or the HTM.

$$\frac{1}{\tau_n} = \frac{1}{\tau_{r1}} + \frac{1}{\tau_{r2}} \tag{1}$$

$$\frac{1}{\tau_{r1}} = k_{r1}Q^+ \tag{2}$$

For this model, we focus on τ_{r1}, which will have the strongest dependence on QD size. τ_{r1} is a function of the corresponding rate constant, k_{r1}, and the concentration of oxidized quantum dots, Q^+, as seen in eq 2. Q^+ will depend on the rate constant of the regeneration step, k_{reg}. Hole transfer for regeneration is treated as having an Arrhenius dependence with an activation energy, $E_{VB} - \mu$, associated with the transition-state energy level μ that the hole has to overcome when moving from the valence band level of the QD, E_{VB}, to the spiro-OMeTAD HOMO level, as shown in eq 3. Here, k_B is the Boltzmann constant, T is the temperature, and A is the frequency factor.

$$k_{reg} = Ae^{-(E_{VB} - \mu)/(k_B T)} \tag{3}$$

Equation 3 explains the decrease in recombination with increasing QD size (raising E_{VB} levels) if we assume that the transition-state energy level μ is constant, so that an increase in E_{VB} translates to decreased k_{reg} and decreased amount of oxidized QDs, Q^+, to recombine with. As we do not know the absolute values of the frequency factor or the activation energy, we can determine only shifts in recombination lifetimes relative to a known change in recombination parameters, in order to cancel out both A and μ. The change in recombination lifetime of the case of interest, τ_n, relative to the base case, τ_n^0, is normalized by the change in the recombination lifetime from another known point, τ_n', relative to the base case, as shown in eq 4. This normalization allows τ_n to be simplified to depend on relative shifts in E_{VB} and known parameters of k_B, the Boltzmann constant, and T, the temperature.

$$\frac{\dfrac{1}{\tau_n} - \dfrac{1}{\tau_n^0}}{\dfrac{1}{\tau_n'} - \dfrac{1}{\tau_n^0}} = \frac{e^{-(E_{VB} - E_{VB}^0)/(k_B T)} - 1}{e^{-(E_{VB}' - E_{VB}^0)/(k_B T)} - 1} \tag{4}$$

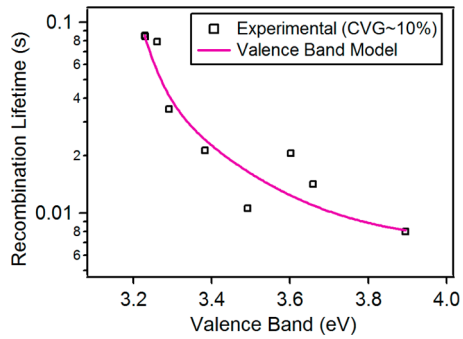

Figure 9. Predicted dependence of recombination lifetimes from the valence band model, eq 4. Experimental recombination lifetimes at V_{OC} of 0.37 V are plotted against the calculated QD valence band level. Included samples are for 4, 6, and 8 SILAR deposition cycles with base-assisted growth (NaOH, ED, and TEA). These samples had similar QD coverages of the TiO_2 surface (coverage ~10%), but varied in QD size, and thus valence band position.

The full derivation is included in the Supporting Information and assumes that τ_{r2} in eq 1 is unchanging. Figure 9 plots the experimental recombination lifetimes *versus* E_{VB} for the NaOH, ED, and TEA devices with 4, 6, or 8 SILAR deposition cycles, which were found to have approximately the same QD coverage (~10.5%). The E_{VB} values (listed in Supporting Information Table S2) were determined from reports of PbS QD band positions at a given size,[84] using the average QD diameters measured from TEM. As these devices all had the same coverage, we are interested to see if, assuming the shifts in recombination lifetime are due only to changes in the QD E_{VB} level, the proposed model can predict the relative shifts in lifetime values. Accordingly, the shortest lifetime value (8-cycle TEA) was chosen as τ_n' and the longest lifetime value (4-cycle TEA) was chosen as τ_n^0. With the high and low points of the model thus pinned, we look at whether the intermediate values follow the dependency predicted by the model. It can be seen that this model well describes the dependence of recombination lifetime on E_{VB}, leading to the conclusion that the increased rates of recombination observed with increased QD size could indeed be due to the upward shift of the QD VB that slows regeneration of the QD by hole transfer to spiro-OMeTAD.

One question remains: whether the longer recombination lifetimes could be caused in the case of ED and TEA by the adsorption of these bases onto the TiO_2 surface. ED or TEA molecules attached to the TiO_2 surface could act to passivate dangling bonds on the TiO_2, reducing trapping of electrons at TiO_2 surface states; in addition, the presence of ED or TEA on the TiO_2 surface could inhibit electrons leaving the TiO_2 to recombine with spiro-OMeTAD. To determine whether adsorption of the base onto the TiO_2 surface was helping to lengthen recombination lifetimes, substrates were prepared with QDs grown by the standard deposition process and then dipped in 1 M TEA aqueous solution after QD growth was complete (referred to as a

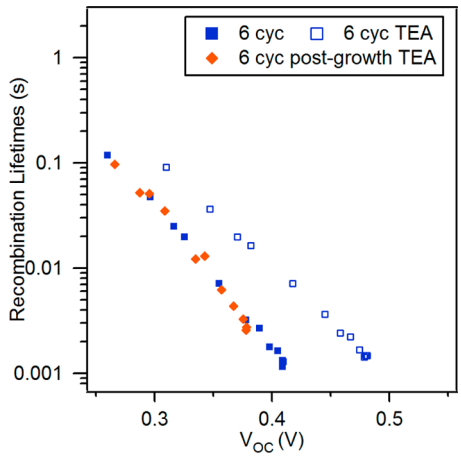

Figure 10. Recombination lifetimes of QDs grown for 6 SILAR cycles by the standard process (6 cycle) and by TEA-assisted QD growth (6-cycle TEA), as compared to QDs grown by the standard process with a post-QD-growth TEA treatment (6-cycle postgrowth TEA).

postgrowth TEA treatment). Data are presented at 6 SILAR cycles, as this gives the optimal device efficiency for the standard deposition process, and if TEA adsorbed on the TiO_2 surface is acting to reduce recombination, a postgrowth TEA treatment should further improve the performance of the standard process. Figure 10 compares the recombination lifetimes of the standard process, TEA-assisted QD growth, and postgrowth TEA treatment. The corresponding *J*−*V* curves and EQE spectra can be found in Supporting Information Figure S7. It can be seen that performance of the postgrowth TEA treatment is almost identical to that of the standard process, in the *J*−*V*, EQE, and recombination lifetime performance. Yet, devices with TEA-assisted QD growth had longer recombination lifetimes. This shows that the longer recombination lifetimes observed with TEA-assisted QD growth are a result of changes in the QD deposition due to TEA, rather than changes due to the presence of TEA on the TiO_2 surface. This conclusion is further supported by the fact that the longer recombination lifetimes observed with ED and TEA in Figure 8a were also observed with NaOH-assisted QD growth. While the presence of NaOH during QD growth led to quantitatively similar increases in QD deposition compared to ED and TEA, NaOH does not introduce ligands into the system that can bind to the TiO_2 surface.

CONCLUSIONS

The loading of PbS QDs on nanoporous TiO_2 substrates is significantly enhanced by controlling the pH of the cation solution during SILAR deposition. A roughly 3-fold increase in QD loading at 2 SILAR cycles is achieved by growing QDs at pH 9 when using three different bases—NaOH, ED, or TEA—indicating that the changes in QD deposition are due primarily to the change in pH, rather than side chemical reactions involving the ligands ED or TEA. The higher QD loading leads to increased device efficiency of solid-state QDSSCs, doubling the efficiency from an average of 0.32% by the standard process to an average of 0.64% with base-assisted QD growth. We found that higher QD loadings lead to recombination lifetimes that are longer by over an order of magnitude. The possibility of surface-adsorbed base molecules impacting recombination was ruled out, leading us to conclude that the improved recombination lifetimes with each base are due to the higher QD coverage of the TiO_2 surface effectively blocking TiO_2 electrons from recombining with the HTM. The net result of higher QD loading is increased light absorption and decreased interfacial recombination, both of which can contribute to higher efficiencies. The QDs also grow in size with increased deposition, which, for cases where QD coverage was constant, was found to give higher interfacial recombination. Our proposed mechanism for the increased recombination with QD size is that the upward shift in the QD valence band in larger QDs inhibits hole transfer from the oxidized QD to the HTM, thus boosting the concentration of oxidized QDs and increasing the recombination of TiO_2 electrons to oxidized QDs. A kinetic model of the effects of QD size is proposed and provides a good explanation of the dependence of recombination lifetimes on size, though further work on a variety of QD materials is needed to fully substantiate this model.

Despite this indication that QD-mediated recombination processes (*e.g.*, electrons from TiO_2 to oxidized QDs) can be significant, the net effect of increased QD loading is decreased interfacial recombination, due to reduced TiO_2−HTM contact, and thus higher charge collection efficiencies. To the authors' knowledge, this constitutes the first report separating the impact on recombination rates of QD loading and QD size in QDSSCs, two variables that usually increase simultaneously during QD deposition. These results identify the mechanisms by which increased QD deposition impacts device performance and clarify that the decline in device efficiencies at higher QD deposition is due to changes in QD size rather than an increase in the number of QDs present. If QD size can be carefully controlled while pushing to near-complete coverage of the TiO_2 surface, we believe QDSSC device efficiencies can be increased into a new regime and may emerge as a competitive thin film photovoltaic technology.

METHODS

TiO_2 Film Deposition. Solid-state QDSSCs were fabricating according to a previous procedure.[85] For the transparent electrode, glass substrates coated with fluorine-doped tin oxide (15 Ω/□, Pilkington) were patterned by etching with 4 M HCl and Zn powder. Substrates were then coated with a thin (~50 nm)

compact layer of TiO_2 by aerosol spray pyrolysis at 450 °C using air as a carrier gas, with titanium diisopropoxide bis-(acetylacetonate) (Sigma 325252) diluted in ethanol as the precursor. The nanoporous TiO_2 layer was then deposited by doctor-blading a commercial paste of 20 nm diameter anatase TiO_2 particles in ethyl cellulose and terpineol (Dyesol 18-NRT), which was diluted with additional terpineol at a 1:1 weight ratio of the commercial paste to terpineol. The films were annealed at 450 °C, resulting in a film thickness of ~2.2 μm as measured by a Dektak profilometer. The nanoporous TiO_2 films were immersed overnight in a 0.02 M aqueous $TiCl_4$ solution at room temperature and then annealed again at 450 °C, to complete the $TiCl_4$ treatment that is standard in DSSC devices.

QD Growth. Lead sulfide quantum dots were grown by SILAR employing 0.02 M aqueous $Pb(NO_3)_2$ (Sigma-Aldrich 11520) as the cation solution (pH 4.3) and 0.02 M aqueous Na_2S (Sigma-Aldrich 407410) as the anion solution (pH 12.3). Nanoporous TiO_2 films were dipped in the cation solution for 2 min, rinsed in DI water for 1 min, then dipped in the anion solution for 2 min, followed by a final dip in DI water for 1 min. For the base-assisted QD growth, NaOH, ethylenediamine (Sigma-Aldrich 03550), and triethanolamine (Sigma 90279) were added to separate solutions of the 0.02 M aqueous $Pb(NO_3)_2$. For NaOH and ED, each was added dropwise to the $Pb(NO_3)_2$ solution to avoid precipitation of PbO, until a pH of 9 was reached. In the case of TEA, a final concentration of 1 M TEA was aimed for, giving a slightly higher pH of 9.2. Care was taken to maintain these pH values (as measured by pH meter) throughout sequential SILAR deposition cycles, through the addition of further base if necessary.

QD Characterization. A Cary 6000i UV−visible spectrophotometer (Varian) was used to characterize the optical properties of the nanoporous TiO_2 film sensitized with PbS QDs. For this study, the nanoporous TiO_2 film was deposited on glass microscope slides. The QDs were also analyzed by transmission electron microscopy (TEM; 200 kV FEI Tecnai G2 F20 X-TWIN). To prepare the TEM samples, material was scraped from QD-covered nanoporous TiO_2 films with an acetone solvent and dispersed on an ultrathin carbon coating on a holey carbon film supported by a 300 mesh copper grid (Ted Pella Inc., #01824). To calculate the average QD size and QD surface coverage of the TiO_2, TEM images were analyzed using ImageJ software. Regions of nonoverlapping TiO_2 nanocrystals were used to calculate surface coverage, by summing the area of all the PbS QDs on that nanocrystal and dividing that by the doubled area of the TiO_2 nanocrystal, as QDs visible in the TEM can be attached to the front or back of the TiO_2 nanocrystal. Overall, at least six TEM images were analyzed for each sample, corresponding to roughly 0.03 μm^2 of TiO_2 surface area and 300 QDs.

Device Fabrication. PbS QDs were deposited on nanoporous TiO_2 substrates by SILAR. As described elsewhere,[35] the solution of the solid-state hole-transporting material was composed of 225 mg mL^{-1} of spiro-OMeTAD (Lumtec LT-S922) dissolved in chlorobenzene, with *tert*-butylpyridine added at a ratio of 1:10.3 μL:mg of spiro-OMeTAD, and lithium bis-(trifluoromethylsulfonyl)imide salt (170 mg mL^{-1} in acetonitrile) added at a ratio of 1:4.8 μL:mg of spiro-OMeTAD. A small amount of the spiro-OMeTAD solution (30 μL for 3.75 cm^2 substrates) was deposited onto the TiO_2 substrates at room temperature and spin-coated at 2000 rpm for 30 s. Finally, 200 nm thick Ag counter electrodes were deposited by thermal evaporation under vacuum below 10^{-6} Torr. Device areas were defined by a combination of an FTO etch line and the metal top contact, and the top metal contact. Final device areas were on the order of 0.1 cm^2, varying slightly from device to device based on the exact position of the FTO etch line with respect to the top contact. The area for each device was measured by an optical microscope. Devices were stored inside a desiccator prior to electrical measurements.

Electrical Measurements. For $J-V$ measurements, an AM 1.5 solar simulator (Oriel 91160) equipped with a 300 W ozone-free Xe arc lamp (6258) was used. The lamp was calibrated to 1 sun (100 mW cm^{-2}) using a reference NREL calibrated Si photodiode equipped with an IR cutoff filter. Current−voltage ($J-V$) curves were collected with a Keithley 2400 SourceMeter, with a sweep delay of 40 ms. Devices were light-soaked until maximum efficiencies were reached (up to 1 h), as was previously found necessary.[63,85] The increase in efficiency with exposure to light is due to doping of the spiro-OMeTAD by oxygen molecules from the atmosphere and is induced by current flow in the device.[86,87] The lower J_{SC} values of these devices explain why the process is slower than the analogous one in DSSCs employing spiro-OMeTAD, which occurs on the time scale of 10 min.[88,89] Representative light-soaking data are included in the Supporting Information, Figure S5. Dark curves were measured after the light-soaking process.

External quantum efficiency measurements were taken at short circuit using monochromated white light from a 100 W tungsten lamp, which was focused through a monochromator. The monochromated illumination, chopped at 40 Hz, was applied in addition to a constant bias light illumination from a white LED array. The photocurrent of the device at each wavelength was acquired through a lock-in amplifier, and the EQE was calculated by referencing the photocurrent from the device to the current from a NIST traceable calibration photodiode.

Transient photovoltage measurements, developed by O'Regan *et al.*,[83,90] were performed at open-circuit voltage (V_{OC}) conditions, following a previously used procedure.[89] A Keithley 2400 source meter was used to maintain the device at zero current. Measurements were taken at different V_{OC} values for a single device by changing the incident bias light. A programmable power supply was used to adjust the white LED array bias light from 0.01 to ~1 sun. A white LED pulse light driven by a function generator (Agilent) was adjusted to approximately 5% of the bias light intensity. The decay of the V_{OC} when the pulsed light turned off was tracked by an oscilloscope (Tektronix). The pulse length was varied from 50 ms to 5 s as necessary to capture the full decay of the V_{OC}. The decay in the V_{OC} was fitted to a single-exponential curve to extract a time constant, which is the recombination lifetime.

Conflict of Interest: The authors declare no competing financial interest.

Supporting Information Available: The Supporting Information is available free of charge on the ACS Publications website at DOI: 10.1021/acsnano.5b02853.

UV−vis spectroscopy, QD size and coverage values, $J-V$ curves, and device performance parameters for the full data set of the standard and NaOH, ED, and TEA conditions at all SILAR cycles, as well as details of the recombination lifetime model (PDF)

Acknowledgment. The PbS QD growth and device fabrication were supported by the Center on Nanostructuring for Efficient Energy Conversion (CNEEC) at Stanford University, an Energy Frontier Research Center funded by the U.S. Department of Energy, Office of Science, Office of Basic Energy Sciences, under Award No. DE-SC0001060. Advanced materials characterization of the PbS QDs (TEM) and advanced device characterization (EQE and transient photovoltage measurements) were supported by the U.S. Department of Energy through the Bay Area Photovoltaic Consortium under Award No. DE-EE0004946. We would like to thank Mike McGehee for his generous sharing of lab equipment and solar cell fabrication procedures, and Thomas Brennan, Colin Bailie, Eric Hoke, and George Margulis for help setting up the transient photovoltage and photocurrent measurement system. We further thank Pralay Santra and Axel Palmstrom for their input on interfacial recombination processes.

REFERENCES AND NOTES

1. O'Regan, B.; Grätzel, M. A Low-Cost, High-Efficiency Solar Cell Based on Dye-Sensitized Colloidal TiO_2 Films. *Nature* **1991**, *353*, 737–740.
2. Roelofs, K. E.; Brennan, T. P.; Bent, S. F. Interface Engineering in Inorganic-Absorber Nanostructured Solar Cells. *J. Phys. Chem. Lett.* **2014**, *5*, 348–360.
3. Kamat, P. V. Quantum Dot Solar Cells: The Next Big Thing in Photovoltaics. *J. Phys. Chem. Lett.* **2013**, *4*, 908–918.

4. Rühle, S.; Shalom, M.; Zaban, A. Quantum-Dot-Sensitized Solar Cells. *ChemPhysChem* **2010**, *11*, 2290–2304.
5. Mora-Seró, I.; Bisquert, J. Breakthroughs in the Development of Semiconductor-Sensitized Solar Cells. *J. Phys. Chem. Lett.* **2010**, *1*, 3046–3052.
6. Hetsch, F.; Xu, X.; Wang, H.; Kershaw, S. V.; Rogach, A. L. Semiconductor Nanocrystal Quantum Dots as Solar Cell Components and Photosensitizers: Material, Charge Transfer, and Separation Aspects of Some Device Topologies. *J. Phys. Chem. Lett.* **2011**, *2*, 1879–1887.
7. Peter, L. M. The Grätzel Cell: Where Next? *J. Phys. Chem. Lett.* **2011**, *2*, 1861–1867.
8. Yu, W. W.; Qu, L.; Guo, W.; Peng, X. Experimental Determination of the Extinction Coefficient of CdTe, CdSe, and CdS Nanocrystals. *Chem. Mater.* **2003**, *15*, 2854–2860.
9. Meng, K.; Surolia, P. K.; Byrne, O.; Thampi, K. R. Efficient CdS Quantum Dot Sensitized Solar Cells Made Using Novel Cu_2S Counter Electrode. *J. Power Sources* **2014**, *248*, 218–223.
10. Lee, H.; Wang, M.; Chen, P.; Gamelin, D. R.; Zakeeruddin, S. M.; Grätzel, M.; Nazeeruddin, M. K. Efficient CdSe Quantum Dot-Sensitized Solar Cells Prepared by an Improved Successive Ionic Layer Adsorption and Reaction Process. *Nano Lett.* **2009**, *9*, 4221–4227.
11. Wang, J.; Mora-Seró, I.; Pan, Z.; Zhao, K.; Zhang, H.; Feng, Y.; Yang, G.; Zhong, X.; Bisquert, J. Core/Shell Colloidal Quantum Dot Exciplex States for the Development of Highly Efficient Quantum-Dot-Sensitized Solar Cells. *J. Am. Chem. Soc.* **2013**, *135*, 15913–15922.
12. Sung, S. D.; Lim, I.; Kang, P.; Lee, C.; Lee, W. I. Design and Development of Highly Efficient PbS Quantum Dot-Sensitized Solar Cells Working in an Aqueous Polysulfide Electrolyte. *Chem. Commun.* **2013**, *49*, 6054–6056.
13. McDaniel, H.; Fuke, N.; Makarov, N. S.; Pietryga, J. M.; Klimov, V. I. An Integrated Approach to Realizing High-Performance Liquid-Junction Quantum Dot Sensitized Solar Cells. *Nat. Commun.* **2013**, *4*, 2887.
14. Pan, Z.; Mora-Seró, I.; Shen, Q.; Zhang, H.; Li, Y.; Zhao, K.; Wang, J.; Zhong, X.; Bisquert, J. High-Efficiency "Green" Quantum Dot Solar Cells. *J. Am. Chem. Soc.* **2014**, *136*, 9203–9210.
15. Duan, J.; Tang, Q.; He, B.; Yu, L. Efficient In_2S_3 Quantum Dot-Sensitized Solar Cells: A Promising Power Conversion Efficiency of 1.30%. *Electrochim. Acta* **2014**, *139*, 381–385.
16. O'Mahony, F. T. F.; Lutz, T.; Guijarro, N.; Gomez, R.; Haque, S. A. Electron and Hole Transfer at Metal Oxide/Sb_2S_3/Spiro-OMeTAD Heterojunctions. *Energy Environ. Sci.* **2012**, *5*, 9760–9764.
17. Zhao, K.; Pan, Z.; Mora-Seró, I.; Cánovas, E.; Wang, H.; Song, Y.; Gong, X.; Wang, J.; Bonn, M.; Bisquert, J.; *et al.* Boosting Power Conversion Efficiencies of Quantum-Dot-Sensitized Solar Cells Beyond 8% by Recombination Control. *J. Am. Chem. Soc.* **2015**, *137*, 5602–5609.
18. Yella, A.; Lee, H.-W.; Tsao, H. N.; Yi, C.; Chandiran, A. K.; Nazeeruddin, M. K.; Diau, E. W.-G.; Yeh, C.-Y.; Zakeeruddin, S. M.; Grätzel, M. Porphyrin-Sensitized Solar Cells with Cobalt (II/III)−Based Redox Electrolyte Exceed 12% Efficiency. *Science* **2011**, *334*, 629–634.
19. Jean, J.; Brown, P. R.; Jaffe, R. L.; Buonassisi, T.; Bulovic, V. Pathways for Solar Photovoltaics. *Energy Environ. Sci.* **2015**, *8*, 1200–1219.
20. Briscoe, J.; Dunn, S. Extremely Thin Absorber Solar Cells Based on Nanostructured Semiconductors. *Mater. Sci. Technol.* **2011**, *27*, 1741–1756.
21. Lee, M. M.; Teuscher, J.; Miyasaka, T.; Murakami, T. N.; Snaith, H. J. Efficient Hybrid Solar Cells Based on Meso-Superstructured Organometal Halide Perovskites. *Science* **2012**, *338*, 643–647.
22. Heo, J. H.; Im, S. H.; Noh, J. H.; Mandal, T. N.; Lim, C.-S.; Chang, J. A.; Lee, Y. H.; Kim, H.-J.; Sarkar, A.; K, N.; *et al.* Efficient Inorganic-Organic Hybrid Heterojunction Solar Cells Containing Perovskite Compound and Polymeric Hole Conductors. *Nat. Photonics* **2013**, *7*, 486–491.
23. Park, N.-G. Organometal Perovskite Light Absorbers Toward a 20% Efficiency Low-Cost Solid-State Mesoscopic Solar Cell. *J. Phys. Chem. Lett.* **2013**, *4*, 2423–2429.
24. Snaith, H. J. Perovskites: The Emergence of a New Era for Low-Cost, High-Efficiency Solar Cells. *J. Phys. Chem. Lett.* **2013**, *4*, 3623–3630.
25. Boix, P. P.; Larramona, G.; Jacob, A.; Delatouche, B.; Mora-Seró, I.; Bisquert, J. Hole Transport and Recombination in All-Solid Sb_2S_3-Sensitized TiO_2 Solar Cells Using CuSCN As Hole Transporter. *J. Phys. Chem. C* **2012**, *116*, 1579–1587.
26. Bach, U.; Lupo, D.; Comte, P.; Moser, J. E.; Weissortel, F.; Salbeck, J.; Spreitzer, H.; Grätzel, M. Solid-State Dye-Sensitized Mesoporous TiO_2 Solar Cells with High Photon-to-Electron Conversion Efficiencies. *Nature* **1998**, *395*, 583–585.
27. Snaith, H. J.; Schmidt-Mende, L. Advances in Liquid-Electrolyte and Solid-State Dye-Sensitized Solar Cells. *Adv. Mater.* **2007**, *19*, 3187–3200.
28. Wolden, C. A.; Kurtin, J.; Baxter, J. B.; Repins, I.; Shaheen, S. E.; Torvik, J. T.; Rockett, A. A.; Fthenakis, V. M.; Aydil, E. S. Photovoltaic Manufacturing: Present Status, Future Prospects, and Research Needs. *J. Vac. Sci. Technol., A* **2011**, *29*, 030801.
29. Wang, X.; Kurdgelashvili, L.; Byrne, J.; Barnett, A. The Value of Module Efficiency in Lowering the Levelized Cost of Energy of Photovoltaic Systems. *Renewable Sustainable Energy Rev.* **2011**, *15*, 4248–4254.
30. Fthenakis, V.; Alsema, E. Photovoltaics Energy Payback Times, Greenhouse Gas Emissions and External Costs: 2004−Early 2005 Status. *Prog. Photovoltaics* **2006**, *14*, 275–280.
31. Snaith, H. J. Solid-State Dye-Sensitized Solar Cells with Molecular Hole Transporters. In *Dye-Sensitized Solar Cells*; Kalyanasundaram, K., Ed.; CRC Press: Boca Raton, FL, 2010.
32. Pagliaro, M.; Ciriminna, R.; Palmisano, G. Flexible Solar Cells. *ChemSusChem* **2008**, *1*, 880–891.
33. Docampo, P.; Tiwana, P.; Sakai, N.; Miura, H.; Herz, L.; Murakami, T.; Snaith, H. J. Unraveling the Function of an MgO Interlayer in Both Electrolyte and Solid-State SnO_2 Based Dye-Sensitized Solar Cells. *J. Phys. Chem. C* **2012**, *116*, 22840–22846.
34. Li, T. C.; Goes, M. S.; Fabregat-Santiago, F.; Bisquert, J.; Bueno, P. R.; Prasittichai, C.; Hupp, J. T.; Marks, T. J. Surface Passivation of Nanoporous TiO_2 via Atomic Layer Deposition of ZrO_2 for Solid-State Dye-Sensitized Solar Cell Applications. *J. Phys. Chem. C* **2009**, *113*, 18385–18390.
35. Leijtens, T.; Ding, I. K.; Giovenzana, T.; Bloking, J. T.; McGehee, M. D.; Sellinger, A. Hole Transport Materials with Low Glass Transition Temperatures and High Solubility for Application in Solid-State Dye-Sensitized Solar Cells. *ACS Nano* **2012**, *6*, 1455–1462.
36. Lee, H.; Leventis, H. C.; Moon, S. J.; Chen, P.; Ito, S.; Haque, S. A.; Torres, T.; Nuesch, F.; Geiger, T.; Zakeeruddin, S. M.; *et al.* PbS and CdS Quantum Dot-Sensitized Solid-State Solar Cells: "Old Concepts, New Results". *Adv. Funct. Mater.* **2009**, *19*, 2735–2742.
37. Jun, H. K.; Careem, M. A.; Arof, A. K. Quantum Dot-Sensitized Solar Cells-Perspective and Recent Developments: A Review of Cd Chalcogenide Quantum Dots as Sensitizers. *Renewable Sustainable Energy Rev.* **2013**, *22*, 148–167.
38. Mora-Seró, I.; Giménez, S.; Fabregat-Santiago, F.; Gómez, R.; Shen, Q.; Toyoda, T.; Bisquert, J. Recombination in Quantum Dot Sensitized Solar Cells. *Acc. Chem. Res.* **2009**, *42*, 1848–1857.
39. Hodes, G. Comparison of Dye- and Semiconductor-Sensitized Porous Nanocrystalline Liquid Junction Solar Cells. *J. Phys. Chem. C* **2008**, *112*, 17778–17787.
40. Handa, S.; Wietasch, H.; Thelakkat, M.; Durrant, J. R.; Haque, S. A. Reducing Charge Recombination Losses in Solid State Dye Sensitized Solar Cells: the Use of Donor-Acceptor Sensitizer Dyes. *Chem. Commun.* **2007**, 1725–1727.
41. Palomares, E.; Martinez-Diaz, M. V.; Haque, S. A.; Torres, T.; Durrant, J. R. State Selective Electron Injection in Non-Aggregated Titanium Phthalocyanine Sensitised Nanocrystalline TiO_2 Films. *Chem. Commun.* **2004**, 2112–2113.

42. Pellegrin, Y.; Le Pleux, L.; Blart, E.; Renaud, A.; Chavillon, B.; Szuwarski, N.; Boujtita, M.; Cario, L.; Jobic, S.; Jacquemin, D.; *et al*. Ruthenium Polypyridine Complexes as Sensitizers in NiO Based p-Type Dye-Sensitized Solar Cells: Effects of the Anchoring Groups. *J. Photochem. Photobiol., A* **2011**, *219*, 235–242.
43. Hagberg, D. P.; Yum, J.-H.; Lee, H.; De Angelis, F.; Marinado, T.; Karlsson, K. M.; Humphry-Baker, R.; Sun, L.; Hagfeldt, A.; Grätzel, M.; *et al*. Molecular Engineering of Organic Sensitizers for Dye-Sensitized Solar Cell Applications. *J. Am. Chem. Soc.* **2008**, *130*, 6259–6266.
44. Guijarro, N.; Lana-Villarreal, T.; Mora-Seró, I. n.; Bisquert, J.; Gó mez, R. CdSe Quantum Dot-Sensitized TiO_2 Electrodes: Effect of Quantum Dot Coverage and Mode of Attachment. *J. Phys. Chem. C* **2009**, *113*, 4208–4214.
45. Vogel, R.; Pohl, K.; Weller, H. Sensitization of Highly Porous, Polycrystalline TiO_2 Electrodes by Quantum Sized CdS. *Chem. Phys. Lett.* **1990**, *174*, 241–245.
46. Toyoda, T.; Kobayashi, J.; Shen, Q. Correlation between Crystal Growth and Photosensitization of Nanostructured TiO_2 Electrodes Using Supporting Ti Substrates by Self-Assembled CdSe Quantum Dots. *Thin Solid Films* **2008**, *516*, 2426–2431.
47. Hod, I.; González-Pedro, V.; Tachan, Z.; Fabregat-Santiago, F.; Mora-Seró, I.; Bisquert, J.; Zaban, A. Dye *versus* Quantum Dots in Sensitized Solar Cells: Participation of Quantum Dot Absorber in the Recombination Process. *J. Phys. Chem. Lett.* **2011**, *2*, 3032–3035.
48. Sewvandi, G. A.; Chen, C.; Ishii, T.; Kusunose, T.; Tanaka, Y.; Nakanishi, S.; Feng, Q. Interplay between Dye Coverage and Photovoltaic Performances of Dye-Sensitized Solar Cells Based on Organic Dyes. *J. Phys. Chem. C* **2014**, *118*, 20184–20192.
49. Tachibana, Y.; Haque, S. A.; Mercer, I. P.; Durrant, J. R.; Klug, D. R. Electron Injection and Recombination in Dye Sensitized Nanocrystalline Titanium Dioxide Films: A Comparison of Ruthenium Bipyridyl and Porphyrin Sensitizer Dyes. *J. Phys. Chem. B* **2000**, *104*, 1198–1205.
50. Guijarro, N.; Campina, J. M.; Shen, Q.; Toyoda, T.; Lana-Villarreal, T.; Gomez, R. Uncovering the Role of the ZnS Treatment in the Performance of Quantum Dot Sensitized Solar Cells. *Phys. Chem. Chem. Phys.* **2011**, *13*, 12024–12032.
51. González-Pedro, V.; Xu, X.; Mora-Seró, I.; Bisquert, J. Modeling High-Efficiency Quantum Dot Sensitized Solar Cells. *ACS Nano* **2010**, *4*, 5783–5790.
52. McDaniel, H.; Fuke, N.; Pietryga, J. M.; Klimov, V. I. Engineered $CuInSe_xS_{2-x}$ Quantum Dots for Sensitized Solar Cells. *J. Phys. Chem. Lett.* **2013**, *4*, 355–361.
53. Markus, T. Z.; Itzhakov, S.; Alkotzer, Y. I.; Cahen, D.; Hodes, G.; Oron, D.; Naaman, R. Energetics of CdSe Quantum Dots Adsorbed on TiO_2. *J. Phys. Chem. C* **2011**, *115*, 13236–13241.
54. Watson, D. F. Linker-Assisted Assembly and Interfacial Electron-Transfer Reactivity of Quantum Dot-Substrate Architectures. *J. Phys. Chem. Lett.* **2010**, *1*, 2299–2309.
55. Mora-Seró, I.; Giménez, S.; Moehl, T.; Fabregat-Santiago, F.; Lana-Villareal, T.; Gómez, R.; Bisquert, J. Factors Determining the Photovoltaic Performance of a CdSe Quantum Dot Sensitized Solar Cell: the Role of the Linker Molecule and of the Counter Electrode. *Nanotechnology* **2008**, *19*, 424007.
56. Wang, H.; McNellis, E. R.; Kinge, S.; Bonn, M.; Cánovas, E. Tuning Electron Transfer Rates through Molecular Bridges in Quantum Dot Sensitized Oxides. *Nano Lett.* **2013**, *13*, 5311–5315.
57. Salant, A.; Shalom, M.; Hod, I.; Faust, A.; Zaban, A.; Banin, U. Quantum Dot Sensitized Solar Cells with Improved Efficiency Prepared Using Electrophoretic Deposition. *ACS Nano* **2010**, *4*, 5962–5968.
58. Salant, A.; Shalom, M.; Tachan, Z.; Buhbut, S.; Zaban, A.; Banin, U. Quantum Rod-Sensitized Solar Cell: Nanocrystal Shape Effect on the Photovoltaic Properties. *Nano Lett.* **2012**, *12*, 2095–2100.
59. Chang, J. A.; Im, S. H.; Lee, Y. H.; Kim, H.-J.; Lim, C.-S.; Heo, J. H.; Seok, S. I. Panchromatic Photon-Harvesting by Hole-Conducting Materials in Inorganic−Organic Heterojunction Sensitized-Solar Cell through the Formation of Nanostructured Electron Channels. *Nano Lett.* **2012**, *12*, 1863–1867.
60. Shalom, M.; Dor, S.; Rühle, S.; Grinis, L.; Zaban, A. Core/CdS Quantum Dot/Shell Mesoporous Solar Cells with Improved Stability and Efficiency Using an Amorphous TiO_2 Coating. *J. Phys. Chem. C* **2009**, *113*, 3895–3898.
61. Sarkar, S. K.; Kim, J. Y.; Goldstein, D. N.; Neale, N. R.; Zhu, K.; Elliott, C. M.; Frank, A. J.; George, S. M. In_2S_3 Atomic Layer Deposition and Its Application as a Sensitizer on TiO_2 Nanotube Arrays for Solar Energy Conversion. *J. Phys. Chem. C* **2010**, *114*, 8032–8039.
62. Brennan, T. P.; Ardalan, P.; Lee, H.-B.-R.; Bakke, J. R.; Ding, I. K.; McGehee, M. D.; Bent, S. F. Atomic Layer Deposition of CdS Quantum Dots for Solid-State Quantum Dot Sensitized Solar Cells. *Adv. Energy Mater.* **2011**, *1*, 1169–1175.
63. Brennan, T. P.; Trejo, O.; Roelofs, K. E.; Xu, J.; Prinz, F. B.; Bent, S. F. Efficiency Enhancement of Solid-State PbS Quantum Dot-Sensitized Solar Cells with Al_2O_3 Barrier Layer. *J. Mater. Chem. A* **2013**, *1*, 7566–7571.
64. Pathan, H. M.; Lokhande, C. D. Deposition of Metal Chalcogenide Thin Films by Successive Ionic Layer Adsorption and Reaction (SILAR) Method. *Bull. Mater. Sci.* **2004**, *27*, 85–111.
65. Baker, D. R.; Kamat, P. V. Photosensitization of TiO_2 Nanostructures with CdS Quantum Dots: Particulate versus Tubular Support Architectures. *Adv. Funct. Mater.* **2009**, *19*, 805–811.
66. Zeng, Q.; Kong, X.; Sun, Y.; Zhang, Y.; Tu, L.; Zhao, J.; Zhang, H. Synthesis and Optical Properties of Type II CdTe/CdS Core/Shell Quantum Dots in Aqueous Solution via Successive Ion Layer Adsorption and Reaction. *J. Phys. Chem. C* **2008**, *112*, 8587–8593.
67. Chi, C.-F.; Chen, P.; Lee, Y.-L.; Liu, I. P.; Chou, S.-C.; Zhang, X.-L.; Bach, U. Surface Modifications of CdS/CdSe Co-Sensitized TiO_2 Photoelectrodes for Solid-State Quantum-Dot-Sensitized Solar Cells. *J. Mater. Chem.* **2011**, *21*, 17534–17540.
68. Jun, H. K.; Careem, M. A.; Arof, A. K. Fabrication, Characterization, and Optimization of CdS and CdSe Quantum Dot-Sensitized Solar Cells with Quantum Dots Prepared by Successive Ionic Layer Adsorption and Reaction. *Int. J. Photoenergy* **2014**, *2014*, 14.
69. Liu, I. P.; Chang, C.-W.; Teng, H.; Lee, Y.-L. Performance Enhancement of Quantum-Dot-Sensitized Solar Cells by Potential-Induced Ionic Layer Adsorption and Reaction. *ACS Appl. Mater. Interfaces* **2014**, *6*, 19378–19384.
70. Edri, E.; Rabinovich, E.; Niitsoo, O.; Cohen, H.; Bendikov, T.; Hodes, G. Uniform Coating of Light-Absorbing Semiconductors by Chemical Bath Deposition on Sulfide-Treated ZnO Nanorods. *J. Phys. Chem. C* **2010**, *114*, 13092–13097.
71. Lee, J.-W.; Hong, J.-D.; Park, N.-G. Sixfold Enhancement of Photocurrent by Surface Charge Controlled High Density Quantum Dot Coating. *Chem. Commun.* **2013**, *49*, 6448–6450.
72. Guijarro, N.; Lana-Villarreal, T.; Shen, Q.; Toyoda, T.; Gómez, R. Sensitization of Titanium Dioxide Photoanodes with Cadmium Selenide Quantum Dots Prepared by SILAR: Photoelectrochemical and Carrier Dynamics Studies. *J. Phys. Chem. C* **2010**, *114*, 21928–21937.
73. Wang, H.; Barceló, I.; Lana-Villarreal, T.; Gómez, R.; Bonn, M.; Cánovas, E. Interplay Between Structure, Stoichiometry, and Electron Transfer Dynamics in SILAR-based Quantum Dot-Sensitized Oxides. *Nano Lett.* **2014**, *14*, 5780–5786.
74. Thielsch, R.; Böhme, T.; Reiche, R.; Schläfer, D.; Bauer, H. D.; Böttcher, H. Quantum-Size Effects of PbS Nanocrystallites in Evaporated Composite Films. *Nanostruct. Mater.* **1998**, *10*, 131–149.
75. Kosmulski, M. The Significance of the Difference in the Point of Zero Charge Between Rutile and Anatase. *Adv. Colloid Interface Sci.* **2002**, *99*, 255–264.
76. Robel, I.; Kuno, M.; Kamat, P. V. Size-Dependent Electron Injection from Excited CdSe Quantum Dots into TiO_2 Nanoparticles. *J. Am. Chem. Soc.* **2007**, *129*, 4136–4137.

77. Leventis, H. C.; O'Mahony, F.; Akhtar, J.; Afzaal, M.; O'Brien, P.; Haque, S. A. Transient Optical Studies of Interfacial Charge Transfer at Nanostructured Metal Oxide/PbS Quantum Dot/Organic Hole Conductor Heterojunctions. *J. Am. Chem. Soc.* **2010**, *132*, 2743–2750.
78. Yang, Y.; Rodríguez-Córdoba, W.; Xiang, X.; Lian, T. Strong Electronic Coupling and Ultrafast Electron Transfer between PbS Quantum Dots and TiO_2 Nanocrystalline Films. *Nano Lett.* **2012**, *12*, 303–309.
79. Pijpers, J. J. H.; Koole, R.; Evers, W. H.; Houtepen, A. J.; Boehme, S.; de Mello Donegá, C.; Vanmaekelbergh, D.; Bonn, M. Spectroscopic Studies of Electron Injection in Quantum Dot Sensitized Mesoporous Oxide Films. *J. Phys. Chem. C* **2010**, *114*, 18866–18873.
80. Guijarro, N.; Shen, Q.; Giménez, S.; Mora-Seró, I.; Bisquert, J.; Lana-Villarreal, T.; Toyoda, T.; Gómez, R. Direct Correlation between Ultrafast Injection and Photoanode Performance in Quantum Dot Sensitized Solar Cells. *J. Phys. Chem. C* **2010**, *114*, 22352–22360.
81. Makarov, N. S.; McDaniel, H.; Fuke, N.; Robel, I.; Klimov, V. I. Photocharging Artifacts in Measurements of Electron Transfer in Quantum-Dot-Sensitized Mesoporous Titania Films. *J. Phys. Chem. Lett.* **2014**, *5*, 111–118.
82. O'Regan, B. C.; Scully, S.; Mayer, A. C.; Palomares, E.; Durrant, J. The Effect of Al_2O_3 Barrier Layers in TiO_2/Dye/CuSCN Photovoltaic Cells Explored by Recombination and DOS Characterization Using Transient Photovoltage Measurements. *J. Phys. Chem. B* **2005**, *109*, 4616–4623.
83. Barnes, P. R. F.; Miettunen, K.; Li, X.; Anderson, A. Y.; Bessho, T.; Grätzel, M.; O'Regan, B. C. Interpretation of Optoelectronic Transient and Charge Extraction Measurements in Dye-Sensitized Solar Cells. *Adv. Mater.* **2013**, *25*, 1881–1922.
84. Hyun, B.-R.; Zhong, Y.-W.; Bartnik, A. C.; Sun, L.; Abruña, H. D.; Wise, F. W.; Goodreau, J. D.; Matthews, J. R.; Leslie, T. M.; Borrelli, N. F. Electron Injection from Colloidal PbS Quantum Dots into Titanium Dioxide Nanoparticles. *ACS Nano* **2008**, *2*, 2206–2212.
85. Roelofs, K. E.; Brennan, T. P.; Dominguez, J. C.; Bailie, C. D.; Margulis, G. Y.; Hoke, E. T.; McGehee, M. D.; Bent, S. F. Effect of Al_2O_3 Recombination Barrier Layers Deposited by Atomic Layer Deposition in Solid-State CdS Quantum Dot-Sensitized Solar Cells. *J. Phys. Chem. C* **2013**, *117*, 5584–5592.
86. Nguyen, W. H.; Bailie, C. D.; Unger, E. L.; McGehee, M. D. Enhancing the Hole-Conductivity of Spiro-OMeTAD without Oxygen or Lithium Salts by Using Spiro$(TFSI)_2$ in Perovskite and Dye-Sensitized Solar Cells. *J. Am. Chem. Soc.* **2014**, *136*, 10996–11001.
87. Yang, L.; Xu, B.; Bi, D.; Tian, H.; Boschloo, G.; Sun, L.; Hagfeldt, A.; Johansson, E. M. J. Initial Light Soaking Treatment Enables Hole Transport Material to Outperform Spiro-OMeTAD in Solid-State Dye-Sensitized Solar Cells. *J. Am. Chem. Soc.* **2013**, *135*, 7378–7385.
88. Brennan, T. P.; Bakke, J. R.; Ding, I. K.; Hardin, B. E.; Nguyen, W. H.; Mondal, R.; Bailie, C. D.; Margulis, G. Y.; Hoke, E. T.; Sellinger, A.; *et al*. The Importance of Dye Chemistry and $TiCl_4$ Surface Treatment in the Behavior of Al_2O_3 Recombination Barrier Layers Deposited by Atomic Layer Deposition in Solid-State Dye-Sensitized Solar Cells. *Phys. Chem. Chem. Phys.* **2012**, *14*, 12130–12140.
89. Brennan, T. P.; Tanskanen, J. T.; Roelofs, K. E.; To, J. W. F.; Nguyen, W. H.; Bakke, J. R.; Ding, I. K.; Hardin, B. E.; Sellinger, A.; McGehee, M. D.; *et al*. TiO_2 Conduction Band Modulation with In_2O_3 Recombination Barrier Layers in Solid-State Dye-Sensitized Solar Cells. *J. Phys. Chem. C* **2013**, *117*, 24138–24149.
90. O'Regan, B. C.; Lenzmann, F. Charge Transport and Recombination in a Nanoscale Interpenetrating Network of n-Type and p-Type Semiconductors: Transient Photocurrent and Photovoltage Studies of TiO_2/Dye/CuSCN Photovoltaic Cells. *J. Phys. Chem. B* **2004**, *108*, 4342–4350.